Global and Planetary Change 221 (2023) 104053

Contents lists available at ScienceDirect

Global and Planetary Change

journal homepage: www.elsevier.com/locate/gloplacha

Effects of carbonate minerals and exogenous acids on carbon flux from the chemical weathering of granite and basalt

Chaojun Li [a,b], Pete Smith [c], Xiaoyong Bai [a,d,*], Qiu Tan [e], Guangjie Luo [f], Qin Li [a,g], Jinfeng Wang [a,g], Luhua Wu [a,g], Fei Chen [a,g], Yuanhong Deng [a], Zeyin Hu [a], Yujie Yang [a], Shiqi Tian [a], Qian Lu [a], Huipeng Xi [a], Chen Ran [a], Sirui Zhang [a]

[a] State Key Laboratory of Environmental Geochemistry, Institute of Geochemistry, Chinese Academy of Sciences, Guiyang 550081, Guizhou Province, China
[b] University of Chinese Academy of Sciences, Beijing 100049, China
[c] Institute of Biological and Environmental Sciences, University of Aberdeen, 23 St Machar Drive, Aberdeen AB24 3UU, United Kingdom
[d] CAS Center for Excellence in Quaternary Science and Global Change, Xi'an 710061, Shanxi Province, China
[e] School of Geography and Environmental Sciences, Guizhou Normal University, Guiyang 550001, China
[f] Guizhou Provincial Key Laboratory of Geographic State Monitoring of Watershed, Guizhou Education University, Guiyang 550018, China
[g] Puding Karst Ecosystem Observation and Research Station, Chinese Academy of Sciences, Puding 562100, Guizhou Province, China

ARTICLE INFO

Editor: Dr. Alan Haywood

Keywords:
Carbonate minerals
Rock weathering
Carbon sink
Silicate
Climate change

ABSTRACT

The chemical weathering of silicate rocks can yield bicarbonate which is transported via rivers to the ocean, followed by the deposition of carbonate, acting as a carbon sink on long time scales. The dissolution of carbonate minerals and the participation of exogenous acids (e.g., sulfuric acid and nitric acid) also affect the chemical weathering process. However, their effects have rarely been quantified at the global scale. Here, based on a compilation of time series datasets of hydro-chemistry samples from 3573 monitoring sites and high-resolution hydro-meteorological datasets, we quantified the effects of carbonate minerals and exogenous acids on the carbon fluxes from the chemical weathering of granite and basalt. The calculated true carbon fluxes of the chemical weathering of granite and basalt were approximately 28.72 Tg C/yr and 30.42 Tg C/yr on the global grid scale. Although the effects of exogenous acids to the true carbon fluxes of the chemical weathering from granite and basalt were similar, corresponding to 30% and 28% of the estimated cation fluxes, respectively, the effect of carbonate minerals on the chemical weathering of granite was approximately twice the effect on the chemical weathering of basalt. These discrepancies were caused by the differences in the chemical weathering characteristics and the laws that integrated the different effects of basalt and granite. Our results address the roles of carbonate minerals and exogenous acids in the global carbon cycle and their link to CO_2 consumption via the chemical weathering of silicate rocks.

1. Introduction

The chemical weathering of silicate rocks can absorb atmospheric and soil CO_2 and can form a negative feedback mechanism with climate change on geological time scales (Berner et al., 1983; Ebelmen, 1845; Walker et al., 1981). As a stabilizer of the evolution of geological systems, the chemical weathering of silicate rocks (e.g. granite and basalt) also releases key biological nutrients that are conducive to plant growth, further drawing down additional atmospheric CO_2 (Chadwick et al., 1999; Hartmann et al., 2013; Vicca et al., 2022). Therefore, chemical weathering of silicate rocks plays a critical role in the global nutrient cycle, environmental changes, and even in the energy balance of the Earth's surface on long time scales (Bai et al., 2023; Ibarra et al., 2016; Xiong et al., 2022).

At present, numerous attempts have been made to evaluate the rates of the chemical weathering of silicate rocks and the associated fluxes of carbon sinks at the regional and global scales (Caldeira, 1992; Caves Rugenstein et al., 2016; Mackenzie and Garrels, 1971; Maher and Chamberlain, 2014). Exogenous acids and carbonate minerals are believed as to have important effect on the estimations of the carbon

* Corresponding author at: State Key Laboratory of Environmental Geochemistry, Institute of Geochemistry, Chinese Academy of Sciences, Guiyang 550081, Guizhou Province, China
E-mail address: baixiaoyong@vip.skleg.cn (X. Bai).

https://doi.org/10.1016/j.gloplacha.2023.104053
Received 28 March 2022; Received in revised form 25 January 2023; Accepted 27 January 2023
Available online 29 January 2023

fluxes of the chemical weathering of silicate rocks (Bufe et al., 2021; Hilton and West, 2020; Jacobson and Blum, 2000; Kanzaki et al., 2020; Liu and Han, 2020; Torres et al., 2016). In addition, carbonate minerals refer to calcite and dolomite in the regions primarily consisting of silicate rocks (Capo et al., 2000; Drever and Hurcomb, 1986). Previous studies have suggested that carbonate minerals generally contribute approximately 40–90% to the chemical weathering of silicate rocks (Blum et al., 1998; Jacobson et al., 2002; Jacobson et al., 2015; Mast et al., 1990). The chemical weathering of trace carbonate minerals (accessory calcite) in silicate rocks accelerates the release of excess calcium, thus increasing the overall CO_2 consumption in these areas (White et al., 1999; White et al., 2005). However, some studies have attributed this excess calcium to secondary carbonate phases associated with carbonate rock formation (strata) and carbonate mineral in Quaternary sediments, especially for the rivers with relatively large basin areas (Bickle et al., 2005; Chen et al., 2022).

Furthermore, exogenous acids refer to sulfuric acid and nitric acid from natural inputs and human activities (Hübner, 1986; Perrin et al., 2008; Xu et al., 2021). Specially, sulfuric acid is mainly produced by natural pyrite oxidation and anthropogenic emissions from fossil fuel combustion, while nitric acid is mainly produced by processes such as reduced nitrogen fertilizer oxidation, atmospheric deposition, and microbial nitrification (Kendall, 1998; Lerman et al., 2007; Liu et al., 2018). Exogenous acids (sulfuric and nitric acids) promote the chemical weathering of both silicate and carbonate rocks (Spence and Telmer, 2005; Tranter et al., 2002). However, on long time scales ($>$ 5–10 ka and $<$ 10 Ma), the involvement of exogenous acids may lead to the release of CO_2 into the atmosphere, which in turn counteracts the removal of atmospheric CO_2 during the chemical weathering of silicate rocks (Kemeny et al., 2021; Relph et al., 2021; Torres et al., 2014). Existing studies have suggested that sulfide oxidation may account for 20–48% of the cation flux during the chemical weathering of silicate rocks (Calmels et al., 2011; Das et al., 2012; Galy and France-Lanord, 1999; Liu et al., 2016b). Granite and basalt are the two typical representative types of silicate rocks (Amiotte Suchet and Probst, 1993; Mackenzie and Garrels, 1971; Meybeck, 1987). Numerous studies have explored the granite- and basalt-related CO_2 consumption fluxes, patterns, and driving factors at different spatial scales (Hartmann et al., 2014; Ibarra et al., 2016; Taylor et al., 2015; Zhang et al., 2021). Numerous efforts have been made to account for the effects of sulfide oxidation and carbonate minerals on silicate chemical weathering (Bufe et al., 2021; Ferris et al., 1994; Torres et al., 2014). However, effectively quantifying the effects of exogenous acids and trace carbonate minerals on the chemical weathering on a global scale remains challenging in granite- and basalt-dominated regions. This is mainly due to the limitations of the in hydro-chemistry data and methods, as well as the interaction of multiple environmental factors. Nevertheless, the resolution of this issue is crucial to effectively assessing the true carbon sink potential of the chemical weathering of granite and basalt.

In this study, we compiled a hydro-chemical database and a spatial hydro-meteorological database and designed a systematic research workflow (Fig. S1). The primary research goals of this study were to estimate the magnitudes of the CO_2 consumption fluxes and cation fluxes of the chemical weathering of granite and basalt and to quantify the effects of carbonate minerals and exogenous acids on the CO_2 consumption fluxes of the chemical weathering of granite and basalt. The results of this study will provide insights into the effects of exogenous acids and carbonate minerals on the chemical weathering carbon sinks of granite and basalt, and help to advance carbon cycle studies related to the chemical weathering carbon sinks of silicate rocks.

2. Material and methods

2.1. Data collection and processing

The main ion concentration database ($[Cl^-]$, $[Ca^{2+}]$, $[Mg^{2+}]$, $[Na^+]$, $[K^+]$, $[HCO_3^-]$, and $[SO_4^{2-}]$) of global major catchments compiled in this study comprised three data sources. The first one was provided by the GEMS/Water data center operated by the International Water Resources and Global Change Center. These data were from the United Nations Environment Program (2017), the Global Freshwater Environmental Monitoring System Program (GEMS/Water) GEMStat database, and Koblenz International Water and Global Change Center. The second source was the GLObal RIver CHemistry (GLORICH) database, with approximately 17,000 monitoring sites. The third source was the GEMS-GLORI database, in which hydro-chemistry data from the 555 global rivers were compiled, and the area of every river basin monitored exceeds 10,000 km^2. Given the relative lack of data on NO_3^- concentration in comparison with other major ions, NO_3^- were not considered in this study. Furthermore, based on the above data sources, monitoring data for the concentrations of HCO_3^- (61,557 samples) (1992–2010) were compiled from 3573 monitoring sites (Fig. 1).

Rock samples from the granite (1398 samples) and basalt (5613 samples) (MgO, CaO, Na_2O, Mg, Ca, and Na) came from the Geochemistry Library (ECL) (https://search.earthchem.org/). To reduce the effects of some outlier rock samples, we selected 10% to 90% of all samples, including 1224 samples of granite and 4267 samples of basalt, and calculated the average values of Ca/Na and Mg/Na from this culled dataset (i.e., a trimmed mean). Granite and granodiorite are the primary composition of acid plutonic rocks, accounting for approximately 1/3 and 2/3 (Berner and Berner, 1996), and basalt and andesite are the main composition of basic volcanic rocks, accounting for approximately 1/4 and 3/4 (Dürr et al., 2005; Hartmann and Moosdorf, 2012). Here, both lithological distributions (acid plutonic rocks and basic volcanic rocks) are regarded as the main distributions of granite and basalt. At the watershed scale, we subsampled rock samples of granite and basalt through the global lithology map, and only retained river basins with the area proportion of granite or basalt >0. The entire compilation survived with 130 granite samples and 95 basalt samples after filtering. Meanwhile, to reduce the confounding effects between different lithologies, we performed the analysis under three scenarios, as described in 2.2 Forward model ((e) Calculation of the RCO_2 value). We collected multi-source environmental factors at the global scale (Table S1). These datasets consisted primarily of runoff (q), precipitation (PRE), temperature (TEM), actual evapotranspiration (ET), soil volume water content (SWC), normalized difference vegetation index (NDVI) and digital elevation model (DEM). To make these raster datasets from distinct sources convenient for spatial simulations or predictions, all raster datasets were re-sampled to 25 km. Combined with the period of hydro-chemistry data collected, the research period of this study was from 1992 to 2014.

2.2. Forward model

The forward model initiated by Mackenzie and Garrels (1971) is one of the classical models used to allocate each solute to the dissolution of a rock type following a series of steps based on hydro-chemistry data (Gaillardet et al., 1999; Liu et al., 2016a; Meybeck, 1987). The main calculation steps used in this study are as follows.

(a) Site selection. The compiled global hydro-chemistry monitoring samples were selected according to the lithological map (granite and basalt) and vector boundaries of river basins. The site chemistry data was selected effectively to reduce the effects of the chemical weathering of other rocks.

(b) Sea salt correction. The method of sea salt correction is the primary method used to determine marine aerosol and precipitation chemistry (Keene et al., 1986). The model is carried out to subtract the effects of chloride ions from the atmosphere, which originates from sea salt and human activities (Sherwood, 1989). The correction of the molar concentrations of chloride ions is used ($[Ca^{2+}]/[Cl^-] = 0.019$, $[Mg^{2+}]/[Cl^-] = 0.097$, $[Na^+]/[Cl^-] = 0.859$, $[K^+]/[Cl^-] = 0.019$ and $[HCO_3^-]/[Cl^-] = 0.004$) (Wilson, 1975). Wilson (1975) has shown a low deviation

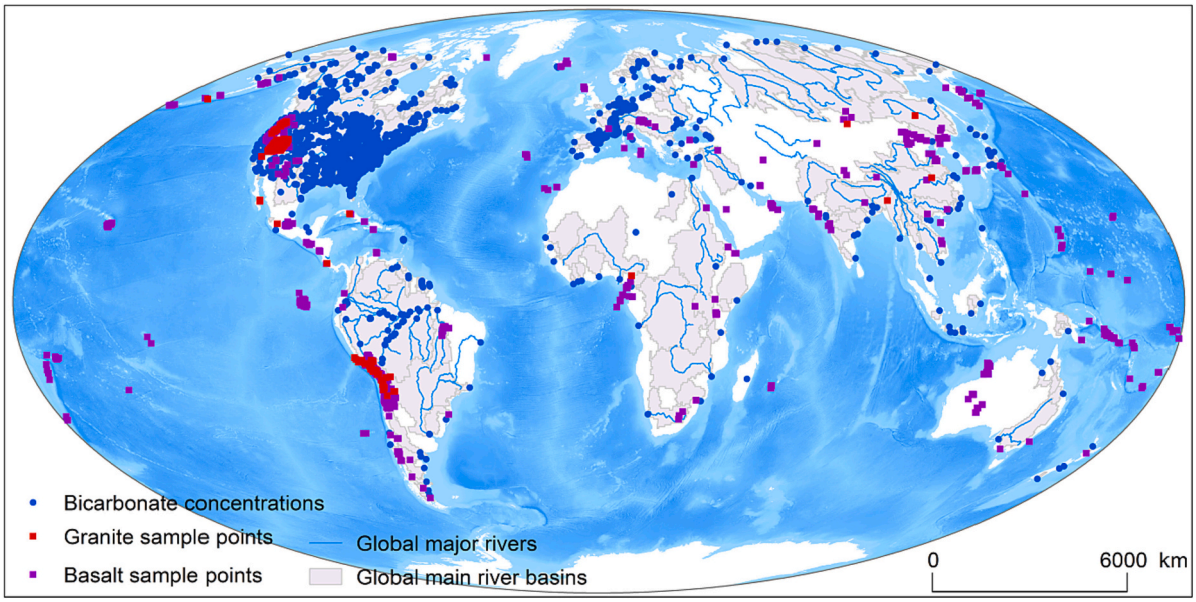

Fig. 1. Compilation of hydro-chemical data in global major river basins and a rock database of granite and basalt. There are 3573 stations (61,557 samples) for HCO_3^- concentration data, rock samples of granite and basalt (7011 samples).

of major ion concentrations in seawater (about 0.1%). As a result, the uncertainties do not need to be considered in the calculation process (Keene et al., 1986). Here, the atmospheric input components were calculated using the [Cl^-] critical approach (Formula (1)) and subtracted from the hydro-chemistry data (Gaillardet et al., 1999). The minimum concentrations of [Cl^-] ([Cl^-]$_{min}$) at each monitoring station was multiplied by a factor from each river basin. The factor represented the effect of evapotranspiration on the concentrations of [Cl^-], and it was calculated by dividing PRE by precipitation minus ET (Grosbois et al., 2000). However, when the values of PRE minus ET were lower than zero, the average concentrations of [Cl^-] in the river basins of the monitoring stations were used instead of the minimum concentrations of [Cl^-].

$$[X]_{atm} = [Cl^-]_{min} \times \frac{PRE}{PRE - ET} \times \left[\frac{X}{Cl^-}\right]_{rain} \quad (1)$$

Wherein, [X]$_{atm}$ means the concentrations of the atmosphere input. And X means major ions ([Ca^{2+}], [Mg^{2+}], [Na^+], [K^+], and [HCO_3^-]). [Cl^-]$_{min}$ means the minimum concentration of [Cl^-]. [Cl^-]$\times\left[\frac{X}{Cl}\right]_{rain}$ means the concentration ratio of the ions mentioned above to concentration of [Cl^-] in rainwater. PRE means precipitation, and ET means actual evapotranspiration.

(c) Subtracting the effect of exogenous acids. The concentrations of cations ([K^+], [Ca^{2+}], [Mg^{2+}], or [Na^+]) might be affected by the chemical weathering of carbonate and silicate rocks through the sulfuric acid (H_2SO_4), nitric acid (HNO_3), as well as carbonic acid (H_2CO_3). Bicarbonate was derived primarily from the chemical weathering of silicate rocks through H_2CO_3, and the chemical weathering of carbonate rocks through H_2CO_3, H_2SO_4, and HNO_3 (Bluth and Kump, 1994; Johnson et al., 1972). After subtracting the part from atmospheric input, the ratio of bicarbonate to the equivalent of main cation (2[Ca^{2+}] + 2[Mg^{2+}] + [K^+] + [Na^+]) could at least effectively subtract the effects of exogenous acids (H_2SO_4 and HNO_3) on the chemical weathering of granite and basalt in this study. In addition, the chemical weathering of carbonate by exogenous acids was not excluded (Han and Liu, 2004; Li et al., 2019a). The specific derivation formula is as follows (Formula (2)).

$$\alpha = \frac{[HCO_3^-]_{riv-atm}}{[Cation]_{riv-atm}} = \frac{[HCO_3^-]^{H_2CO_3}_{sil+carb} + [HCO_3^-]^{H_2SO_4+HNO_3}_{carb}}{[Cation]^{H_2CO_3}_{sil+carb} + [Cation]^{H_2SO_4+HNO_3}_{sil+carb}} \quad (2)$$

Where α means the ratio of bicarbonate ions ([HCO_3^-]) to cations in the river basins after subtracting atmospheric input (*riv-atm*), which is chosen to subtract the effects of some exogenous acids, including the effects of sulfuric acid (H_2SO_4) and nitric acid (HNO_3) on the chemical weathering of rocks. The cation is equivalent to (2[Ca^{2+}] + 2[Mg^{2+}] + [K^+] + [Na^+]), and *sil* and *carb* represent the chemical weathering of silicate (granite and basalt) and carbonate rocks. The α of granite or basalt is calculated separately by this formula (2).

(d) Subtracting the effect of carbonate minerals. As weathering cations may come from carbonate minerals and the chemical weathering of granite and basalt, it is necessary to subtract the effect of carbonate minerals. Here, Ca/Na and Mg/Na of granite and basalt were selected, and the method was called "Ca-Mg excess" (Clow et al., 1997; Hartmann, 2009). Assuming all the remaining [Na^+] came from granite and basalt, and the ratios of Ca/Na and Mg/Na of granite and basalt were relatively stable, the potential concentrations of [Ca^{2+}] and [Mg^{2+}] from the chemical weathering of granite and basalt could be calculated according to the ratios of Ca/Na and Mg/Na of granite and basalt, thus [Ca^{2+}] and [Mg^{2+}] generated by the chemical weathering of carbonate minerals could be subtracted effectively. The concentrations of major ions of the chemical weathering of silicate rocks could be calculated (Formula (3) to (7)). The ratios of Ca/Na and Mg/Na of granite and basalt were calculated using compiled data of rock samples (Table S2). The estimated values of Ca/Na and Mg/Na of granite were 0.87 ± 0.04 and 0.33 ± 0.01, while those of basalt were 2.94 ± 0.09 and 1.77 ± 0.11.

$$[Na^+]_{sil} = \alpha[Na^+]_{riv-atm} \quad (3)$$

$$[K^+]_{sil} = \alpha[K^+]_{riv-atm} \quad (4)$$

$$[Ca^{2+}]_{sil} = [Na^+]_{sil} \times \left(\frac{[Ca^{2+}]}{[Na^+]}\right)_{rock} \quad (5)$$

$$[Mg^{2+}]_{sil} = [Na^+]_{sil} \times \left(\frac{[Mg^{2+}]}{[Na^+]}\right)_{rock} \quad (6)$$

$$[HCO_3^-]_{sil} = [Na^+]_{sil} + [K^+]_{sil} + 2[Ca^{2+}]_{sil} + 2[Mg^{2+}]_{sil} \quad (7)$$

[X]$_{sil}$ refers to the ion concentrations generated by the chemical weathering of silicate rocks (granite and basalt). And X means major

ions ([Ca^{2+}], [Mg^{2+}], [Na^{+}], [K^{+}], and [HCO_3^-]). These ion concentrations of granite or basalt were calculated separately. α refers to the ratio of bicarbonate ions ([HCO_3^-]) to cations in the river basin after subtracting atmospheric input (Formula (2)). $[X]_{riv\text{-}atm}$ refers to the average of the ion concentrations in the river basin via subtracting the concentrations of atmospheric input. $[X]_{rock}$ refers to the weight of ion concentrations in rock samples.

(e) Calculation of the RCO_2value. RCO_2 refers to the ratio of atmospheric CO_2 consumption of granite and basalt to bicarbonate ions in the river basins, which was equal to the ratio of the concentrations of the weathering cations of granite and basalt to the concentrations of total cations. Here, RCO_2 was calculated after subtracting the effects of atmospheric input and exogenous acids (Formula (8)). To reduce the RCO_2 calculation deviation caused by mixing of different lithologies in the river basins, three scenarios were designed in this study: (a) the area proportion of granite and basalt was greater than zero, (b) the area proportion of granite and basalt was >50% and (c) the area proportion of carbonate rock was <0.05, and the area proportion of granite (or basalt) was greater than that of basalt (or granite). Finally, the RCO_2 from the chemical weathering of granite or basalt was calculated, respectively. If there was no interference from other lithologies, the remaining values (1–RCO_2) were considered as the contribution rates to the chemical weathering of carbonate minerals.

$$RCO_2 = \frac{[HCO_3^-]_{sil}^{H_2CO_3}}{\alpha[Cation]_{riv-atm}} = \frac{[Cation]_{sil}^{H_2CO_3}}{[HCO_3^-]_{riv-atm}} \quad (8)$$

$[X]_{sil}^{H_2CO_3}$refers to the ion concentrations ([Cation] and [HCO_3^-]) generated by the chemical weathering of silicate rocks (granite and basalt) via carbonic acid (H_2CO_3). α refers to the ratio of bicarbonate ions ([HCO_3^-]) to cations after subtracting atmospheric input (Formula (2)). [Cation] is the sum of 2[Ca^{2+}], 2[Mg^{2+}], [Na^{+}] and [K^{+}]. $[HCO_3^-]_{riv\text{-}atm}$ is the average of the concentrations ([HCO_3^-]) in the river basins via subtracting the concentrations of atmospheric input.

(f) Calculation of weathering cation fluxes of granite and basalt. After subtracting the effects of the atmosphere input, exogenous acids, and carbonate minerals, we calculated the total weathering cation concentrations of silicate rocks (granite and basalt) (2[Ca^{2+}] + 2[Mg^{2+}] + [K^{+}] + [Na^{+}]). The weathering cation fluxes of granite and basalt were then calculated, respectively.

$$T_{cat-gra} = \left([Na^+]_{gra} + [K^+]_{gra} + 2[Ca^{2+}]_{gra} + 2[Mg^{2+}]_{gra}\right) \times q \times A \quad (9)$$

$$T_{cat-bas} = \left([Na^+]_{bas} + [K^+]_{bas} + 2[Ca^{2+}]_{bas} + 2[Mg^{2+}]_{bas}\right) \times q \times A \quad (10)$$

$T_{cat\text{-}gra}$ and $T_{cat\text{-}bas}$ represent the total fluxes of weathering cations of granite and basalt, with the unit of kg C/yr. $[X]_{gra}$ and $[X]_{bas}$ represent the ions concentrations of major cations produced by the chemical weathering of granite and basalt, with the unit of mg/L. Here, *X* means major ions ([Ca^{2+}], [Mg^{2+}], [Na^{+}], and [K^{+}]). *q* represents the average annual runoff of the river basins, with the unit of mm. *A* represents the area (km^2) of the river basins.

2.3. $FHCO_3^-$-RCO_2 method

According to the data of bicarbonate and chloride ion concentrations compiled from the major stations in the world, the effect of bicarbonate generated by atmospheric inputs to the chemical weathering of rocks was eliminated via the sea salt correction method, and the bicarbonate ion fluxes ($FHCO_3^-$) were calculated via the corrected bicarbonate ion concentrations multiplied by the runoff (*q*). $FHCO_3^-$ was multiplied by the area (*A*) of the regions to calculate the total bicarbonate ion fluxes ($THCO_3^-$). Based on PRE, TEM, ET, *q*, NDVI, and SWC, the spatial distribution of $FHCO_3^-$ at the global scale was simulated by random forest algorithm, and the tenfold cross validation was carried out. This method has been successfully applied to the simulation of spatial ion concentration (Li et al., 2019b; Li et al., 2018).

The random forest method for both classification and regression proposed by Breiman (2001) is a tree-based ensemble algorithm, and it is robust against over-fitting. It has been widely used in the spatial simulation of critical factors (Li et al., 2022; Terrer et al., 2021). We predicted the spatial distribution of $FHCO_3^-$ using random forest regression algorithm (See the Appendix). Moreover, based on $FHCO_3^-$-RCO_2 method (Formula (11) and (12)), we calculated the total fluxes of true CO_2 consumption from the chemical weathering of global granite and basalt.

$$T_{gra} = [HCO_3^-]_{riv-atm} \times RCO_{2gra} \times q \times A = [HCO_3^-]_{gra}^{H_2CO_3} \times q \times A \quad (11)$$

$$T_{bas} = [HCO_3^-]_{riv-atm} \times RCO_{2bas} \times q \times A = [HCO_3^-]_{bas}^{H_2CO_3} \times q \times A \quad (12)$$

Wherein, $[HCO_3^-]_{riv\text{-}atm}$ is the concentrations ([HCO_3^-]) via subtracting the concentrations of atmospheric input, with the unit of mg/L. $RCO_{2gra}$and RCO_{2bas}refer to the ratios of CO_2 consumption from granite and basalt to bicarbonate concentrations (Formula (8)). $[HCO_3^-]_{gra}^{H_2CO_3}and[HCO_3^-]_{bas}^{H_2CO_3}$refer to the ion concentrations generated by the chemical weathering of granite and basalt via carbonic acid (H_2CO_3), with the unit of mg/L. *q* represents the average annual runoff (mm). *A* represents the area (km^2) of granite and basalt.

2.4. West model

The total amount of the chemical weathering of silicate rocks mainly depends on the amount of materials entering the weathering layer, the residence time of minerals in the weathering layer, and the rate of the chemical weathering (Gabet, 2007). Most studies have shown that mineral-supply-limited and kinetically-limited are two important weathering regimes to quantify the relationship between physical erosion and chemical weathering (Gabet and Mudd, 2009; Hilley et al., 2010). Subsequently, a one-dimensional dynamic vertical model has been established by the concept of reactive transport in granitic and granodioritic rocks (West, 2012). This model, named the West model, provides an estimation of the weathering cation in silicate rock areas, which is coupled with climatic conditions and physical erosion rate. The physical erosion rate is calculated by combining the large-scale catchment comprehensive method (BQART model) (Syvitski and Milliman, 2007) with the small-scale river power law (SPIM) (Davy and Crave, 2000; Howard, 1994) (See the Appendix). And the West model has been well applied in silicate rocks around the world (Maffre et al., 2018). The specific formula of the West model is as follows.

$$F_{cat} = \chi_m \bullet E \bullet \left\{1 - exp\left[-K \bullet (1 - exp(-k_w q))\right. \right. \\ \left. \left. \bullet exp\left(-\frac{E_a}{R}\left(\frac{1}{Tk} - \frac{1}{T_0}\right)\right) \bullet \frac{(z/E)^{\sigma+1}}{\sigma+1}\right]\right\} \quad (13)$$

Some parameters of the model and descriptions of the corresponding calculation models are shown in Table S1. Although the ranges of six critical parameters (χ_m, *K*, E_a, k_w, *z*, and $\sigma + 1$) of granite were calculated (West, 2012), but these parameters remained certain uncertainties due to the limitation of observational data. Maffre et al. (2018) fitted six critical parameters in silicate rocks around the world, but the parameters for specific granite and basalt are not distinguished. Therefore, the critical parameter range of basalt may still be unclear. To calculate effectively the fluxes of the weathering cation of granite and basalt on the global scale, we re-estimated the spatial ranges of these parameters based on more hydro-chemical data. Here, we mainly used nonlinear methods (Levenberg-Marquardt (LM) and universal global optimization (UGO) algorithms). LM is a nonlinear optimization method based on the Gauss-Newton method and the gradient descent method, and the solution typically accelerates to the local minimum (Lourakis, 2005; Marquardt, 1963). UGO is the core algorithm of 1stOpt software, which

overcomes the problem that the iterative method must give the initial value, and can effectively obtain the optimal solution. Using 1stOpt software package (http://www.7d-soft.com/en/), we simulated the main parameters based on the LM and UGO algorithms. Finally, we estimated the weathering cation of global granite and basalt ($2[Ca^{2+}] + 2[Mg^{2+}] + [K^{+}] + [Na^{+}]$) by the West model.

2.5. Trend analysis and F-test

The inter-annual variability trends of the chemical weathering of granite and basalt were analyzed by the linear regression method and F-test on the global grid scale. The calculation formula is as follows (Xiao et al., 2023).

$$\theta_{slope} = \frac{n \times \sum_{i=1}^{n}(i \times \tau_i) - \sum_{i=1}^{n} i \sum_{i=1}^{n} \tau_i}{n \times \sum_{i=1}^{n} i^2 - \left(\sum_{i=1}^{n} i\right)^2} \quad (14)$$

In the formula, n is the total number of years ($n = 23$), i is the year ($i = 1, 2, \ldots 23$); and τ_i are the grid values for year i. If θ_{slope} is greater than zero, the overall τ exhibited an increasing trend from 1992 to 2014. The absolute values of the θ_{slope} magnitude represent the strength of the change in τ. To further clarify the spatial distribution patterns of the changes, the F test and significance levels (0.01 and 0.05) were used to divide quantitatively the variability trends. The calculation formula for the F test is as follows.

$$F = \frac{(n-2) \times \sum_{i=1}^{n}(\tau_i - \tau_m)}{\sum_{i=1}^{n}\left(\tau_{i-f\tau_i}\right)^2} \quad (15)$$

Where n is the total number of years ($n = 23$), $f\tau_i$ are the grid values of the corresponding years, and τ_m is the multi-year average. F represents the preliminary calculation result of the F test. By testing the results of F at the significance levels of 0.01 and 0.05, the results are divided into five possible variations, namely extremely significant increase (ES-I) ($P \leq 0.01$), significant increase (S—I) ($P \leq 0.05$), basic stability (B—S) ($P > 0.05$), significant decrease (S—D) ($P \leq 0.05$), and extremely significant decrease (ES-D) ($P \leq 0.01$).

2.6. Calculation method of uncertainty propagation

Detailed analysis of error propagation is conducive to evaluating the accuracy of a calculation and plays an important role in understanding the relative weight of each part of the error sources. The uncertainty propagation method used here is the square root of the sum of squares, which is widely used in error propagation analysis (Karlsson et al., 2021; Li et al., 2018; Wang et al., 2014). The error propagation function of the

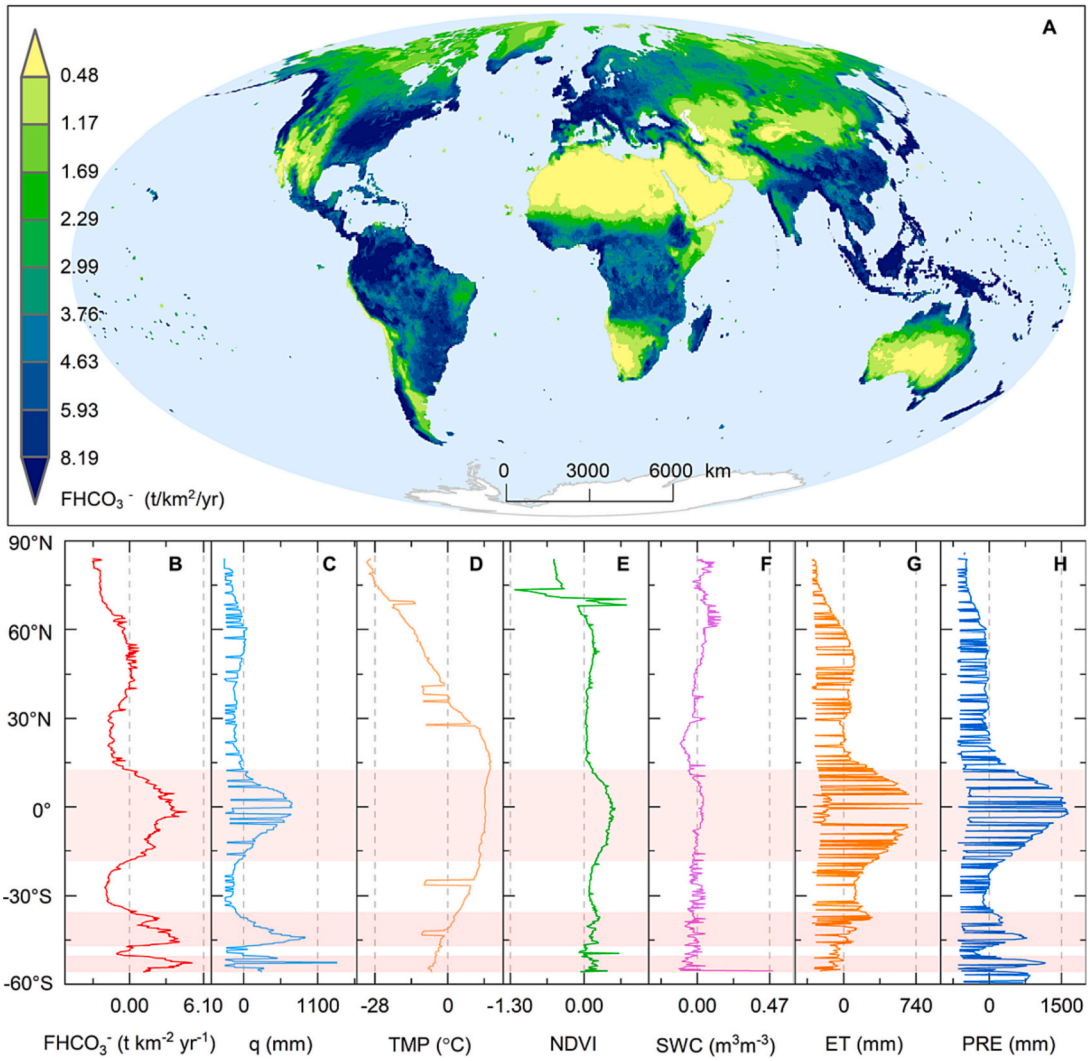

Fig. 2. Spatial distribution of $FHCO_3^-$ flux (A) and the latitudinal anomalies (departure from average) of the main factors: (B) $FHCO_3^-$, (C) q, (D) TEM (TEM = Tk–273.15), (E) NDVI, (F) SWC, (G) ET, and (H) PRE. The pink zones represent the three high anomalies in the latitudinal distribution of the $FHCO_3^-$ flux. (For interpretation of the references to colour in this figure legend, the reader is referred to the web version of this article.)

uncertainty is as follows (Formula (16)).

$$\lambda = \sqrt{\varepsilon^2 + \beta^2 + \gamma^2} \quad (16)$$

In the formula, the final uncertainty (λ) is measured by integrating the fundamental errors in the data sources compiled (ε), simulation method (β) and process analysis (γ), and it is assumed that the errors are mutually independent.

3. Results

3.1. Global CO_2 consumption via the chemical weathering of granite and basalt

Based on the compiled bicarbonate concentration database and the hydro-meteorological spatial database, we simulated the spatial variations in the bicarbonate fluxes ($FHCO_3^-$) at the global scale using the random forest algorithm (Fig. 2). The spatial variations in the $FHCO_3^-$ (mean 3.71 ± 0.19 t/km^2/yr) were primarily controlled by runoff and precipitation. Asia had the largest $THCO_3^-$ value (approximately 0.20 Pg/yr), accounting for 30.43% of the total global amount, and the flux ($FHCO_3^-$) (6.20 ± 0.31 t/km^2/yr) was the highest among all the continents. The maximum of $FHCO_3^-$ values were distributed in the warm temperate zone according to the global Köppen climate types classification (Peel et al., 2007). The flux in the warm temperate zone was approximately six times that in the arid zone, indicating that the moisture content restricted the distribution of the $FHCO_3^-$.

To evaluated the reliability and accuracy of the simulated bicarbonate flux, tenfold cross validation of the observed value and the simulated value was performed (mean R = 0.70, mean RSME = 4.40) (Fig. 3). Based on two indicators (%IncMSE and IncNodePurity), we assessed the relative importance of the factors (Tk, PRE, ET, q, NDVI, and SWC). We found that q, Tk, and SWC were of relatively more important, while PRE, ET, and NDVI were of relatively little importance to the other factors (Fig. 3B). The average of $FHCO_3^-$ flux in North America was 3.56 ± 0.18 t/km^2/yr, which was slightly lower than that reported by Moosdorf et al. (2011) (3.96 ± 0.2 t/km^2/yr). However, the $FHCO_3^-$ flux was 0.62 times higher than that reported by Hartmann (2009) (6.61 t/km^2/yr). Moreover, the average of $FHCO_3^-$ for the Mackenzie Basin (2.54 t/km^2/yr) was very close to the previous results reported by Beaulieu et al. (2012) (1.20–4.03 t/km^2/yr). Compared with the data for 23 major river basins around the world compiled by Cai et al. (2008), we found that our simulation results for the total bicarbonate ion fluxes ($THCO_3^-$) were close to the results for the existing compiled river basins (Fig. S2).

Then, we analyzed and calculated the RCO_2 under three distinctive lithology scenarios (Table S3). The probability densities of the RCO_2 calculation results for granite under the three scenarios were analyzed (Fig. S3). Compared with the first two scenarios ($Gra_{ratio} > 0$ and $Gra_{ratio} > 0.5$), the average of RCO_2 calculated for the third scenario exhibited a nearly normal distribution. Therefore, the RCO_2 value of the chemical weathering of granite (approximately 0.52) calculated for the ($Carb_{ratio} < 0.05$) and ($Gra_{ratio} > Bas_{ratio}$) scenario was finally selected. The second scenario was selected ($Bas_{ratio} > 0.5$) to estimate the basaltic RCO_2 (approximately 0.96). It should be noted that the calculated granitic RCO_2 value was slightly lower than the range of the results (0.58–0.88) estimated by some scholars (Moosdorf et al., 2011). Similarly, we found that it was closer to the basaltic RCO_2 value (0.87–1) calculated using the Ca—Mg excess method (Hartmann, 2009), but the values were within the same range.

We determined the spatial distributions of the carbon fluxes from the chemical weathering of global granite (Fgra) and basalt (Fbas) (Fig. 4), with average values of 2.35 ± 0.95 t/km^2/yr and 4.08 ± 1.66 t/km^2/yr. The Fgra value for South America was the highest among all the continents, with an average of 3.48 ± 0.17 t/km^2/yr. Moreover, the top five countries (Canada, Brazil, Russia, China, and the United States) accounted for 55.15% of the total carbon fluxes from the chemical weathering of granite (Tgra) (Fig. S4). The Tgra value for Canada was mainly attributed to the fraction of its area accounted for by its largest granite area (25.65%). The combined total carbon sink of the chemical weathering of basalt in the top seven countries (i.e., Russia, the United States, India, Brazil, Ethiopia, Canada, and Iceland) was approximately 2.82 ± 1.15 Tg C/yr, accounting for 64.96% of the total global carbon flux from the chemical weathering of basalt.

3.2. Global weathering cation fluxes of granite and basalt

The spatial distribution of the physical erosion rate (E) was very heterogeneous (Fig. S5). Approximately 12.3% of the regions had E values of >500 t/km^2/yr. The total global physical erosion rate was 30.47 Pg/yr from 1992 to 2014. On the river basin scale, there was a correlation between the simulated E value and the monitored E values (R^2 = 0.54, $P < 0.001$) (Milliman, 1995) (Fig. S6). In addition, the best fitting results for Fcat-gra and Fcat-bas demonstrated that the constructed models were effective (R = 0.67, ($P < 0.01$); R = 0.79, ($P < 0.01$)) (Fig. S7). The optimal values of the fitting parameters (χ_m, K, E_a,

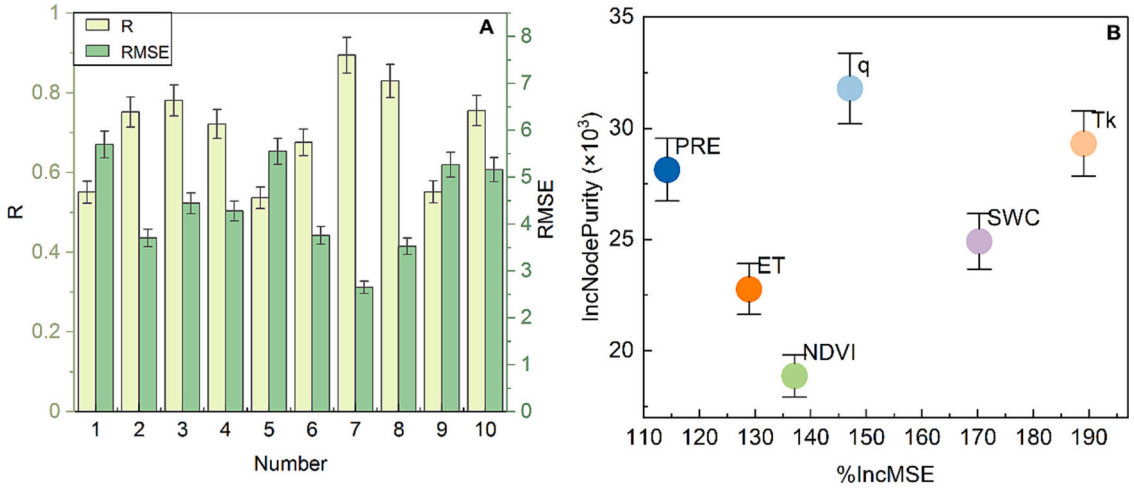

Fig. 3. Verification of calculation results of bicarbonate flux ($FHCO_3^-$). (A) Tenfold cross validation of $FHCO_3^-$ inversion results using random forests method. (B) Evaluation of the relative importance of major predictors. Where %IncMSE is the average reduction value of precision calculated based on out-of-bag (OOB) error rate, which means the importance in the sense of decreasing mean square error, while IncNodePurity is the average reduction value of non-purity of nodes calculated by Gini index, which means the importance in the sense of decreasing residual square sum.

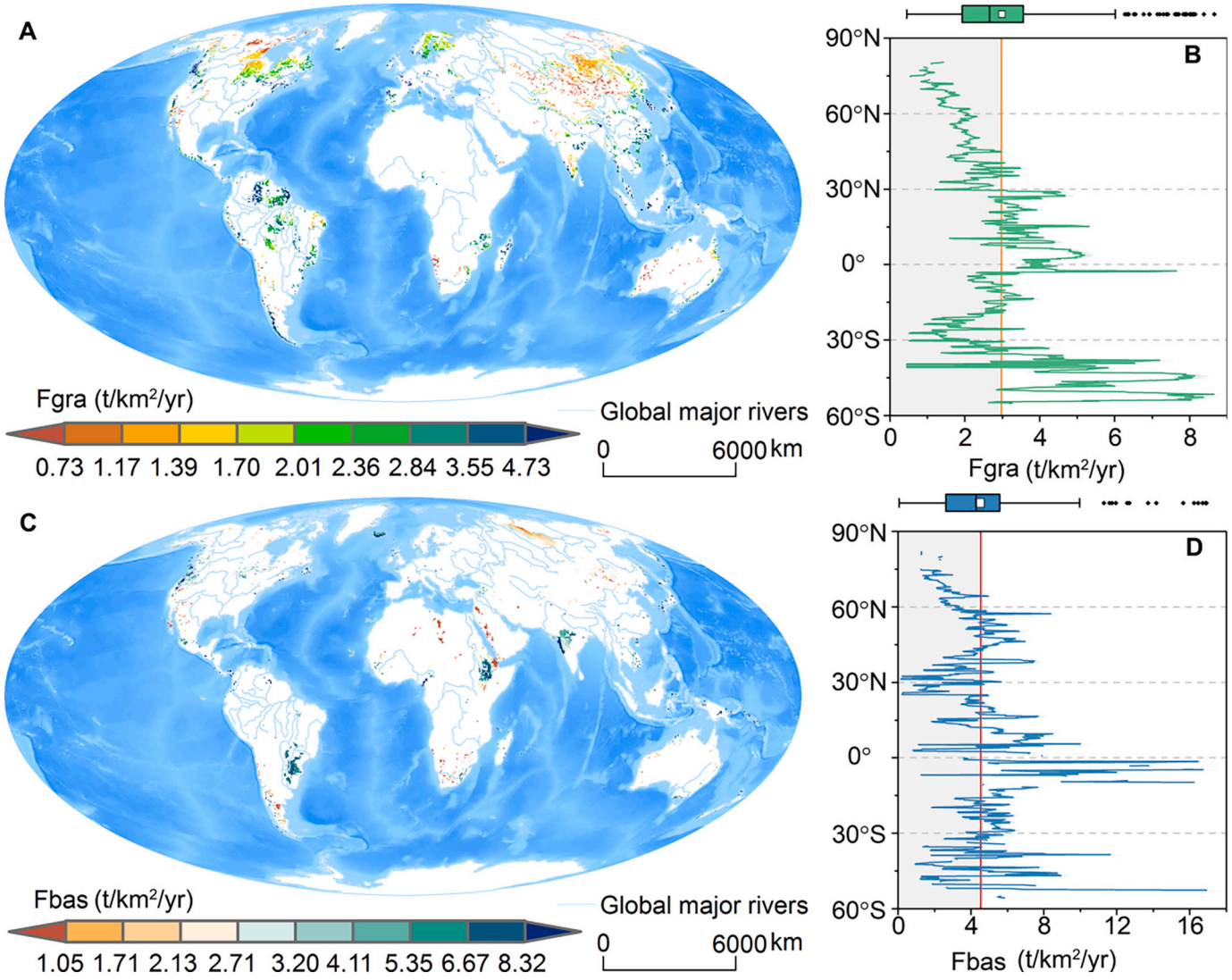

Fig. 4. Spatial and latitudinal variations in the CO_2 consumption caused by chemical weathering of granite (A and B) and basalt (C and D). Fgra means carbon fluxes from the chemical weathering of granite, and Fbas means carbon fluxes from the chemical weathering of basalt. The red lines (B and D) indicate the average fluxes. The upper graphs in B and D are the plots of the latitudinal distributions. (For interpretation of the references to colour in this figure legend, the reader is referred to the web version of this article.)

k_w, z, and $\sigma + 1$) for the chemical weathering of granite were 0.01, 2.99×10^{-3}, 45.04 kJ/mol, 1.79×10^{-4} mm/yr, 9.86×10^{6} t/km^2, and 0.96, respectively (Table S4). The ranges of the six parameters fitted in this study are slightly smaller than the results of West (2012), and they are closer to the results of Maffre et al. (2018). However, the activation energy (E_a) (45.04 kJ/mol) of granite is closest to the results of West (2012). Previous studies have suggested a value of 48.7 kJ/mol (Oliva et al., 2003). The optimal ranges of the six parameters for the chemical weathering of basalt were compared with those of Maffre et al. (2018) (Table S5). We found that the parameter ranges for the carbon sink fluxes of the chemical weathering of basalt were within those ranges reported by Maffre et al. (2018).

Based on the simulation and verification results of the physical erosion rate and the six critical parameters, we mapped the spatial extents of the cation fluxes of the chemical weathering of granite (Fcat-gra) and basalt (Fcat-bas) (Fig. S8). The warm and humid climatic conditions and large topographic relief significantly enhanced the chemical weathering of granite and basalt (Macdonald et al., 2019). By sorting the grid values of the total cation fluxes of the chemical weathering of granite and basalt in descending order and based on analysis of the cumulative percentage areas, we found that 56.25–94.83% of the total cation fluxes of the chemical weathering of granite (Tcat-gra) were distributed within 10–50% of the granite areas (Fig. S9), while approximately 47.19–90.89% of the total cation fluxes of the chemical weathering of basalt (Tcat-bas) were distributed in 10–50% the basalt areas. The correlations between of the weathering cations of granite and basalt and each factor were significantly different (Fig. S10). There was a close correlation between the weathering cation fluxes and E for the granite areas ($R^2 = 0.96$). This may be attributed to physical erosion rate having a greater effect than climate in the granite areas (Riebe et al., 2004; Riebe et al., 2001). However, the correlation between q and Fcat-bas was much larger in the basalt areas ($R^2 = 0.72$) than in the granite areas ($R^2 = 0.26$). This implies that the chemical weathering flux of basalt increases with increasing runoff, which is consistent with the results of previous studies (Hartmann et al., 2009; Ibarra et al., 2016). In addition, we further tested the sensitivities of these factors and found that the Fcat-gra was more sensitive to E, while Fcat-bas was more sensitive to q (Fig. S11). In contrast to the CO_2 consumption fluxes caused by the chemical weathering of granite, the CO_2 consumption fluxes caused by the chemical weathering of basalt slightly decreased from 1992 to 2014 (Fig. S12). It was further determined that the runoff in the basalt areas decreased (−0.26 mm/yr).

3.3. Roles of exogenous acids and carbonate minerals

The contribution rates of exogenous acids to the chemical weathering cation flux of granite and basalt were approximately 30% and 28%, respectively. This indicates that the effects of exogenous acids produced by human activities and pyrite oxidation on the chemical weathering of granite and basalt were similar on average at the global scale. Still, the estimated average value of the effect of exogenous acids on the chemical weathering of granite and basalt was approximately 0.2 ± 0.07 t/km^2/yr at the watershed scale.

In this study, the effect of carbonate minerals was extrapolated to the spatial grid scale (Fig. 5A). The contributions of the carbonate minerals to the chemical weathering of granite and basalt exhibited obvious inconsistencies (Fig. 5B). We found that the highest contribution rate (>90%) of carbonate minerals to the chemical weathering of granite accounted for the largest area proportion, approximately 32.12%, while the lowest contribution rate (<10%) of carbonate minerals to the chemical weathering of basalt accounted for the largest area proportion, approximately 28.44%. Moreover, the average contribution rate of carbonate minerals to the chemical weathering of basalt was approximately 38% (1.2 ± 0.5 t/km^2/yr). In contrast, the global average contribution rate of carbonate minerals to the chemical weathering of granite was 61% (2.41 ± 1.00 t/km^2/yr), which was far greater than the contribution rate of carbonate minerals in the basalt areas. We speculate the main reasons for this were the chemical weathering characteristics and laws of the granite and basalt. The chemical weathering characteristics are mainly reflected by the chemical weathering rate. The chemical weathering rate of basalt is higher than that of granite (Amiotte Suchet et al., 2003; Avila et al., 2022; Balagizi et al., 2015; Dessert et al., 2001; Gislason et al., 1996; Millot et al., 2002). Most studies have discussed the chemical weathering laws of granite and basalt (Dessert et al., 2001; Lasaga et al., 1994; Oliva et al., 2003). We also found that the factors effecting the chemical weathering of granite and basalt were obviously different, that is, basalt was more vulnerable to runoff, and granite may have been more vulnerable to physical erosion (Fig. S10). Owing to the mass balances, the chemical weathering of the granite areas may have been more susceptible to the chemical weathering of carbonate minerals than the basalt areas (Blum et al., 1998; Sverdrup and Warfvinge, 1995).

4. Discussion

4.1. Effects of exogenous acids and carbonate minerals

Exogenous acids, especially sulfuric acid, have a more significant effect on carbonate dissolution than that of silicate rocks (Anderson et al., 2000; Emberson et al., 2018; Liu et al., 2022). Thus, exogenous acids accelerate the chemical weathering of carbonate minerals disseminated in silicate rock areas and may also be associated with the release of CO_2 (Torres et al., 2014). Spence and Telmer (2005) proposed that approximately 48% of the CO_2 consumption during the chemical weathering of silicate rocks may be offset by the CO_2 released via the dissolution of carbonate by sulfuric acid in the Canadian Cordillera, and Relph et al. (2021) estimated that approximately 70% of the CO_2 consumption of that may be offset in the Mekong River Basin. Based on data compiled for major rivers around the world, we found that the contributions of exogenous acids to the chemical weathering cation flux of granite and basalt were similar, approximately 30% and 28%, respectively. These results are comparable with the existing contributions of sulfide oxidation (20–48%) (Calmels et al., 2007; Calmels et al., 2011; Das et al., 2012; Galy and France-Lanord, 1999). We speculated that these similar contributions were largely due to the dissolution of small amounts of carbonate minerals rather than granite or basalt. Further quantification of the effects of different types of acid production may be required in the future. It is important to emphasize the need to effectively exclude the effects of exogenous acids in the assessment of the chemical weathering fluxes of global granite and basalt, as well as in long-term carbon cycle studies (Calmels et al., 2007; Das et al., 2012; Torres et al., 2014).

In addition, carbonate chemical weathering rates are significantly faster than silicate rock chemical weathering rates (Brantley et al., 2008; Tipper et al., 2006; Wolfgang, 2012; Zhang et al., 2019). Based on mass balance calculations, carbonate mineral weathering often dominates the solute fluxes in rivers in silicate regions (Jacobson et al., 2003; Jiang et al., 2018; Oliva et al., 2004; White et al., 1999; White et al., 2005; Zeng et al., 2022). Furthermore, due to the differences in their fracture densities and permeabilities, the chemical weathering rate of basalt is higher than that of granite (Navarre-Sitchler and Brantley, 2007; Worthington et al., 2016). There are also significant differences in the chemical weathering laws of granite and basalt (Dessert et al., 2001; Lasaga et al., 1994; Oliva et al., 2003). Moreover, there are differences in the primary factors influencing the chemical weathering of granite and basalt, that is, basalt is more susceptible to runoff and granite may be more susceptible to physical erosion. Thus, the chemical weathering

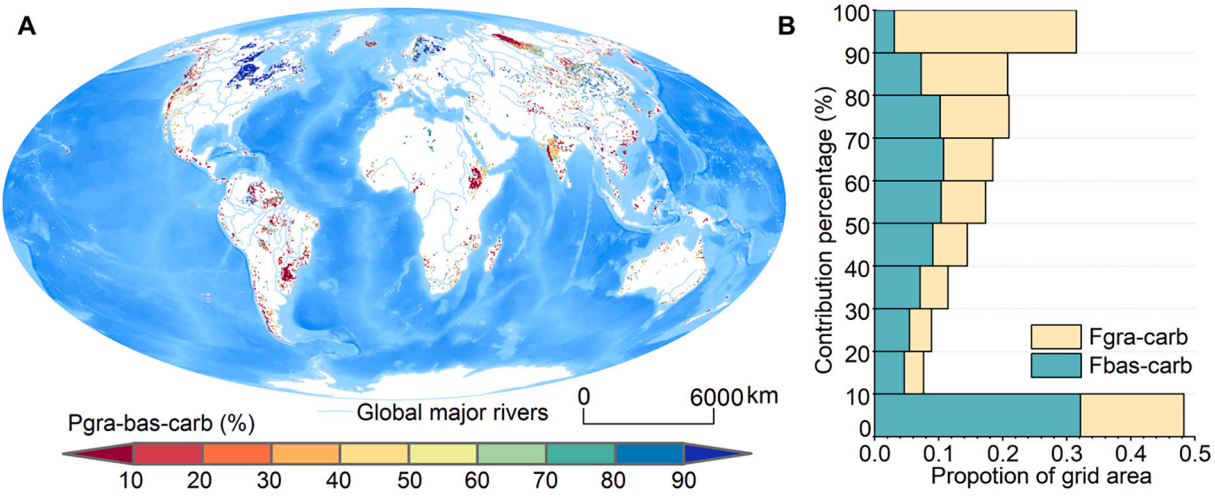

Fig. 5. Effect of carbonate minerals on the chemical weathering of granite and basalt. (A) The effect of carbonate minerals on the chemical weathering of granite and basalt; (B) The contribution percentage of granite and basalt under different grid area.

characteristics and laws may explain the differences in the effects of carbonate minerals on the chemical weathering of basalt and granite identified in this study, with the former being approximately twice as large as the latter. The contributions of carbonate minerals to the chemical weathering of granite and basalt are comparable to existing estimates (Blum et al., 1998; Galy and France-Lanord, 1999; Jacobson et al., 2015; Mast et al., 1990). In conclusion, the accurate quantification of the effects of exogenous acids and carbonate minerals is not only important for the accurate assessment of the carbon sinks of the chemical weathering of silicate rocks, but it also contributes to the accurate quantification of carbon sinks in global terrestrial ecosystems (Ferris et al., 1994; Relph et al., 2021).

4.2. Comparison with previous estimates and prospects for the future

The critical strengths of our study are the exclusion of exogenous acids and carbonate minerals and the estimation of the true CO_2 consumption of the chemical weathering of granite and basalt. To evaluate the reliability of the simulated CO_2 consumption fluxes, we compared them with the results of existing studies (Table S6). The CO_2 consumption fluxes of chemical weathering of granite and basalt were close to those reported in related studies (Dessert et al., 2003; Louvat et al., 2008; Tao et al., 2011). The total CO_2 consumption fluxes of the chemical weathering of granite and basalt were within the total carbon sink range of silicate rock weathering reported in previous studies (Gaillardet et al., 1999; Meybeck, 1987; Moon et al., 2014; Zhang et al., 2021). Furthermore, based on a comparison of the estimated results with those of previous studies on the global net terrestrial carbon sink, the vegetation carbon sink, and the soil carbon sink, we determined that the true carbon sinks from the chemical weathering of granite and basalt (approximately 60 Tg C/yr) are approximately 5% that of the estimated global net vegetation carbon sequestration (approximately 1.1 Pg C/yr) and 4–15% that of the global cultivated land and grassland carbon sink (Lal, 2001; Smith et al., 2008).

However, we noted that there were some differences in the estimated silicate rock areas in previous studies. There were differences in the methods, and the results were slightly different. Thus, it was necessary to analyze the uncertainties and errors propagation. Based on the sensitivity tests, the discharge, limited samples, and inverse model selections for the source differentiation, accounted for approximately 30–40% of the errors in the estimations of the silicate chemical weathering rates on the catchment and global scales in previous studies (Moon et al., 2007; Moquet et al., 2011). Therefore, we estimated a mean uncertainty of 35% for the discharge, limited samples, end-member estimates, and inverse model selections for the source differentiation. In addition, the precise uncertainty of the lithologic map (distribution of basalt and granite) was approximately 5% in this study. The Ca/Na and Mg/Na ratios associated with the chemical weathering of granite and basalt are also related to non-stoichiometric weathering of silicate minerals, especially in kinetically limited regimes where granite and basalt are susceptible to grinding and pulverization (Mitchell and Brown, 2008; Moore et al., 2013; Taylor et al., 2000). Nevertheless, it is currently still difficult to effectively quantify the increase in the cation fluxes of the non-stoichiometric weathering of granite and basalt. Moreover, there may also be the uncertainty in the ion exchange, such as the Na^+ yield of the chemical weathering of basalt and granite (Hodson et al., 2002). Recently, Tipper et al. (2021) found that due to the supplies of Na^+ from large-scale exchange pools with non-silicate origins, the global silicate weathering flux may be overestimated by 12–28%. Here, we calculated the analytical uncertainties as the average of the existing study (approximately 20%). We assumed that the uncertainties discussed above were independent of each other. Using a simple uncertainty propagation method (square root of the sum of squares), we obtained an uncertainty of ±41%.

This uncertainty range is applicable to both the simulation of the magnitudes of the CO_2 consumption of the chemical weathering of granite and basalt. Therefore, the final global carbon sink fluxes of the chemical weathering of granite and basalt were calculated to be 2.35 ± 0.95 t/km^2/yr and 4.08 ± 1.66 t/km^2/yr, respectively. Similarly, we quantified the uncertainties of the propagated errors of the estimation results of the exogenous acids and carbonate minerals, which were 35% and 41%, respectively. Owing to the limitations of the hydro-chemical data, such as the aluminum and potassium concentrations, quantifying the contributions of inconsistent weathering and consistent weathering was difficult in this study. Although considering the main mineral types in granite and basalt were considered in the global lithologic database based on existing research results, precise quantification of the classification purity of the two rock types is lacking, which may depend on the availability of more rock sample data and a higher resolution global lithological map. For future studies, it will be necessary to strengthen both dynamic global river monitoring and hydro-chemical data collection. Furthermore, we need to optimize the model in the future to constrain and distinguish the effects of natural and human related exogenous acids on the chemical weathering carbon sinks of different rocks, and continue to explore the scientific application of machine learning algorithms in the field of the carbon sinks of the chemical weathering of continental rocks.

5. Conclusions

By combining multiple hydro-chemical databases and high-resolution hydro-meteorological spatial datasets, we estimated the true CO_2 consumption during the chemical weathering of granite and basalt and quantified the differences in the contribution rates of exogenous acids and carbonate minerals. The total CO_2 consumption fluxes of the chemical weathering of granite and basalt were estimated to be 28.72 ± 11.67 Tg C/yr and 30.42 ± 12.36 Tg C/yr, respectively. The effects of exogenous acids on the true CO_2 consumption of the chemical weathering of granite and basalt were similar, but the effect of carbonate minerals on the chemical weathering of granite (61%) was approximately twice that of the chemical weathering of basalt (38%). The likely causes of these differences in the chemical weathering characteristics and the differentiation law of granite and basalt. Overall, the results of our study demonstrate that exogenous acids and carbonate minerals are external factors that cannot be ignored in the accurate estimation of the CO_2 consumption of the chemical weathering of silicate rock. In the future, we plan to compile more hydro-chemical data and to optimize the numerical model. In addition, machine learning may become the future direction of carbon sink modeling and understanding of continental rock weathering.

Declaration of Competing Interest

The authors declare that they have no known competing financial interests or personal relationships that could have appeared to influence the work reported in this paper.

Data availability

The hydrochemical datasets related to this article are from the GLObal RIver CHemistry (GLORICH) database (https://doi.pangaea.de/10.1594/PANGAEA.902360), the GEMS-GLORI database (https://doi.pangaea.de/10.1594/PANGAEA.804574) and the GEMS/Water data center. Among them, the hydrochemical data from GEMS/water data center needs to be used by custom data request (https://gemstat.org/custom-data-request/). Rock samples of granite and basalt are from the Geochemistry Library (ECL), and the specific data is stored in PetDB database, which is a searchable database of published geochemical data (https://search.earthchem.org/setsampletype?pkey=3404938).

Acknowledgments

This work was supported jointly by the Western Light Cross-team Program of Chinese Academy of Sciences (No. xbzg-zdsys-202101); National Natural Science Foundation of China (No. 42077455 & No.42167032); Strategic Priority Research Program of the Chinese Academy of Sciences (No. XDB40000000 & No. XDA23060100); Guizhou Provincial Science and Technology Projects (No. Qiankehe Support [2022] General 198); High-level innovative talents in Guizhou Province (No. GCC[2022]015-1 & No. 2016-5648); Guizhou Provincial 2020 Science and Technology Subsidies (No. GZ2020SIG); the Opening Fund of the State Key Laboratory of Environmental Geochemistry (No. SKLEG2022206 & No. SKLEG2022208); and the central government leading local science and technology development (No. QianKeZhongYinDi [2021]4028). We thank the editors and all anonymous reviewers for their constructive comments. Special thanks to Prof. Gaillardet (Institut de Physique du Globe de Paris), Prof. Ibarra (Brown University), and Dr. Bufe (German Research Center for Geosciences (GFZ)) for their constructive suggestions. Thanks to the originator of the hydrochemical datasets acquired through UN Environment GEMS/Water Programme. We thank LetPub (www.letpub.com) for its linguistic assistance during the preparation of this manuscript.

Appendix A. Supplementary data

Supplementary data to this article can be found online at https://doi.org/10.1016/j.gloplacha.2023.104053.

References

Amiotte Suchet, P., Probst, J.L., 1993. Modelling of atmospheric CO_2 consumption by chemical weathering of rocks: Application to the Garonne, Congo and Amazon basins. Chem. Geol. 107 (3), 205–210. https://doi.org/10.1016/0009-2541(93)90174-H.

Amiotte Suchet, P., Probst, J.L., Ludwig, W., 2003. Worldwide distribution of continental rock lithology: Implications for the atmospheric/soil CO_2 uptake by continental weathering and alkalinity river transport to the oceans. Glob. Biogeochem. Cycles 17 (2). https://doi.org/10.1029/2002GB001891.

Anderson, S.P., Drever, J.I., Frost, C.D., Holden, P., 2000. Chemical weathering in the foreland of a retreating glacier. Geochim. Cosmochim. Acta 64 (7), 1173–1189. https://doi.org/10.1016/S0016-7037(99)00358-0.

Avila, T.D., et al., 2022. Role of seafloor production versus continental basalt weathering in Middle to late Ordovician seawater $^{87}Sr/^{86}Sr$ and climate. Earth Planet. Sci. Lett. 593, 117641 https://doi.org/10.1016/j.epsl.2022.117641.

Bai, X., et al., 2023. A carbon neutrality capacity index for evaluating carbon sink contributions. Environ. Sci. Ecotechnol. 100237 https://doi.org/10.1016/j.ese.2023.100237.

Balagizi, C.M., et al., 2015. River geochemistry, chemical weathering, and atmospheric CO_2 consumption rates in the Virunga Volcanic Province (East Africa). Geochem. Geophys. Geosyst. 16 (8), 2637–2660. https://doi.org/10.1002/2015GC005999.

Beaulieu, E., Goddéris, Y., Donnadieu, Y., Labat, D., Roelandt, C., 2012. High sensitivity of the continental-weathering carbon dioxide sink to future climate change. Nat. Clim. Chang. 2 (5), 346–349. https://doi.org/10.1038/nclimate1419.

Berner, E.K., Berner, R.A., 1996. Global Environment: Water, Air and Geochemical Cycles. Prentice Hall, Old Tappan, NJ, United States.

Berner, R.A., Lasaga, A.C., Garrels, R.M., 1983. Carbonate-silicate geochemical cycle and its effect on atmospheric carbon dioxide over the past 100 million years. Am. J. Sci. 283 (7), 641–683. https://doi.org/10.2475/ajs.283.7.641.

Bickle, M.J., et al., 2005. Relative contributions of silicate and carbonate rocks to riverine Sr fluxes in the headwaters of the Ganges. Geochim. Cosmochim. Acta 69 (9), 2221–2240. https://doi.org/10.1016/j.gca.2004.11.019.

Blum, J., Gazis, C., Jacobson, A., Chamberlain, C., 1998. Carbonate verse silicate weathering in the Raikhot watershed within the High Himalayan Crystalline Series. Geology 26. https://doi.org/10.1130/0091-7613(1998)026<0411:CVSWIT>2.3.CO;2.

Bluth, G.J.S., Kump, L.R., 1994. Lithologic and climatologic controls of river chemistry. Geochim. Cosmochim. Acta 58 (10), 2341–2359. https://doi.org/10.1016/0016-7037(94)90015-9.

Brantley, S., Kubicki, J., White, A., Springer, 2008. Kinetics of Water-Rock Interaction.

Breiman, L., 2001. Random forests. Mach. Learn. 45, 5–32. https://doi.org/10.1023/A:1010933404324.

Bufe, A., et al., 2021. Co-variation of silicate, carbonate and sulfide weathering drives CO_2 release with erosion. Nat. Geosci. 14, 211–216. https://doi.org/10.1038/s41561-021-00714-3.

Cai, W., et al., 2008. A comparative overview of weathering intensity and HCO_3^- flux in the world's major rivers with emphasis on the Changjiang, Huanghe, Zhujiang (Pearl) and Mississippi Rivers. Cont. Shelf Res. 28, 1538–1549. https://doi.org/10.1016/j.csr.2007.10.014.

Caldeira, K., 1992. Enhanced Cenozoic chemical weathering and the subduction of pelagic carbonate. Nature 357, 578–580. https://doi.org/10.1038/357578a0.

Calmels, D., Gaillardet, J., Brenot, A., France-Lanord, C., 2007. Sustained sulfide oxidation by physical erosion processes in the Mackenzie River basin: Climatic perspectives. Geology 35, 1003–1006. https://doi.org/10.1130/G24132A.1.

Calmels, D., et al., 2011. Contribution of deep groundwater to the weathering budget in a rapidly eroding mountain belt, Taiwan. Earth Planet. Sci. Lett. 303 (1), 48–58. https://doi.org/10.1016/j.epsl.2010.12.032.

Capo, R.C., Whipkey, C.E., Blachère, J.R., Chadwick, O.A., 2000. Pedogenic origin of dolomite in a basaltic weathering profile, Kohala peninsula, Hawaii. Geology 28 (3), 271–274. https://doi.org/10.1130/0091-7613(2000)28<271:POODIA>2.0.CO;2.

Caves Rugenstein, J., Jost, A., Lau, K., Maher, K., 2016. Cenozoic carbon cycle imbalances and a variable silicate weathering feedback. Earth Planet. Sci. Lett. 450, 152–163. https://doi.org/10.1016/j.epsl.2016.06.035.

Chadwick, O.A., Derry, L.A., Vitousek, P.M., Huebert, B.J., Hedin, L.O., 1999. Changing sources of nutrients during four million years of ecosystem development. Nature 397 (6719), 491–497. https://doi.org/10.1038/17276.

Chen, B.B., et al., 2022. Calcium isotopes tracing secondary mineral formation in the high-relief Yalong River Basin, Southeast Tibetan Plateau. Sci. Total Environ. 827, 154315 https://doi.org/10.1016/j.scitotenv.2022.154315.

Clow, D.W., Mast, M.A., Bullen, T.D., Turk, J.T., 1997. Strontium 87/strontium 86 as a tracer of mineral weathering reactions and calcium sources in an Alpine/Subalpine Watershed, Loch Vale, Colorado. Water Resour. Res. 33 (6), 1335–1351. https://doi.org/10.1029/97WR00856.

Das, A., Chung, C.-H., You, C.-F., 2012. Disproportionately high rates of sulfide oxidation from mountainous river basins of Taiwan orogeny: Sulfur isotope evidence. Geophys. Res. Lett. 39 (12) https://doi.org/10.1029/2012GL051549.

Davy, P., Crave, A., 2000. Upscaling local-scale transport processes in large-scale relief dynamics. Phys. Chem. Earth Solid Earth Geod. 25 (6), 533–541. https://doi.org/10.1016/S1464-1895(00)00082-X.

Dessert, C., et al., 2001. Erosion of Deccan Traps determined by river geochemistry: Impact on the global climate and the $^{87}Sr/^{86}Sr$ ratio of seawater. Earth Planet. Sci. Lett. 188, 459–474. https://doi.org/10.1016/S0012-821X(01)00317-X.

Dessert, C., Dupré, B., Gaillardet, J., François, L.M., Allègre, C.J., 2003. Basalt weathering laws and the impact of basalt weathering on the global carbon cycle. Chem. Geol. 202 (3), 257–273. https://doi.org/10.1016/j.chemgeo.2002.10.001.

Drever, J.I., Hurcomb, D.R., 1986. Neutralization of atmospheric acidity by chemical weathering in an alpine drainage basin in the North Cascade Mountains. Geology 14 (3), 221–224. https://doi.org/10.1130/0091-7613(1986)14<221:NOAABC>2.0.CO;2.

Dürr, H.H., Meybeck, M., Dürr, S.H., 2005. Lithologic composition of the Earth's continental surfaces derived from a new digital map emphasizing riverine material transfer. Glob. Biogeochem. Cycles 19 (4), GB4S10. https://doi.org/10.1029/2005GB002515.

Ebelmen, J.J., 1845. Sur les produits de la décomposition des espèces minérales de la famille des silicates. Ann. Min. 7, 3–66.

Emberson, R., Galy, A., Hovius, N., 2018. Weathering of reactive mineral phases in landslides acts as a source of carbon dioxide in mountain belts. J. Geophys. Res. Earth Surf. 123 (10), 2695–2713. https://doi.org/10.1029/2018JF004672.

Ferris, F.G., Wiese, R.G., Fyfe, W.S., 1994. Precipitation of carbonate minerals by microorganisms: Implications for silicate weathering and the global carbon dioxide budget. Geomicrobiol J. 12 (1), 1–13. https://doi.org/10.1080/01490459409377966.

Gabet, E.J., 2007. A theoretical model coupling chemical weathering and physical erosion in landslide-dominated landscapes. Earth Planet. Sci. Lett. 264 (1), 259–265. https://doi.org/10.1016/j.epsl.2007.09.028.

Gabet, E., Mudd, S., 2009. A theoretical model coupling chemical weathering rate with denudation rates. Geology 37, 151–154. https://doi.org/10.1130/G25270A.1.

Gaillardet, J., Dupré, B., Louvat, P., Allègre, C.J., 1999. Global silicate weathering and CO_2 consumption rates deduced from the chemistry of large rivers. Chem. Geol. 159 (1), 3–30. https://doi.org/10.1016/S0009-2541(99)00031-5.

Galy, A., France-Lanord, C., 1999. Weathering processes in the Ganges–Brahmaputra basin and the riverine alkalinity budget. Chem. Geol. 159 (1), 31–60. https://doi.org/10.1016/S0009-2541(99)00033-9.

Gislason, S., Arnorsson, S., Ármannsson, H., 1996. Chemical weathering of basalt in Southwest Iceland: Effects of runoff, age of rocks and vegetative/glacial cover. Am. J. Sci. 296, 837–907. https://doi.org/10.2475/ajs.296.8.837.

Grosbois, C., Négrel, P., Fouillac, C., Grimaud, D., 2000. Dissolved load of the Loire River: Chemical and isotopic characterization. Chem. Geol. 170, 179–201. https://doi.org/10.1016/S0009-2541(99)00247-8.

Han, G.L., Liu, C.Q., 2004. Water geochemistry controlled by carbonate dissolution: a study of the river waters draining karst-dominated terrain, Guizhou Province, China. Chem. Geol. 204, 1–21. https://doi.org/10.1016/j.chemgeo.2003.09.009.

Hartmann, J., 2009. Bicarbonate-fluxes and CO_2-consumption by chemical weathering on the Japanese Archipelago — Application of a multi-lithological model framework. Chem. Geol. 265 (3), 237–271. https://doi.org/10.1016/j.chemgeo.2009.03.024.

Hartmann, J., Moosdorf, N., 2012. The new global lithological map database (GLiM): a representation of rock properties at the Earth surface. Geochem. Geophys. Geosyst. 13, Q12004 https://doi.org/10.1029/2012GC004370.

Hartmann, J., Jansen, N., Dürr, H.H., Kempe, S., Köhler, P., 2009. Global CO_2-consumption by chemical weathering: what is the contribution of highly active weathering regions? Glob. Planet. Chang. 69 (4), 185–194. https://doi.org/10.1016/j.gloplacha.2009.07.007.

Hartmann, J., et al., 2013. Enhanced chemical weathering as a geoengineering strategy to reduce atmospheric carbon dioxide, supply nutrients, and mitigate ocean acidification. Rev. Geophys. 51 (2), 113–149. https://doi.org/10.1002/rog.20004.
Hartmann, J., Moosdorf, N., Lauerwald, R., Hinderer, M., West, A.J., 2014. Global chemical weathering and associated P-release — the role of lithology, temperature and soil properties. Chem. Geol. 363, 145–163. https://doi.org/10.1016/j.chemgeo.2013.10.025.
Hilley, G., Chamberlain, C., Moon, S., Porder, S., Willett, S., 2010. Competition between erosion and reaction kinetics in controlling silicate-weathering rates. Earth Planet. Sci. Lett. 293, 191–199. https://doi.org/10.1016/j.epsl.2010.01.008.
Hilton, R., West, A.J., 2020. Mountains, erosion and the carbon cycle. Nat. Rev. Earth Environ. 1, 284–299. https://doi.org/10.1038/s43017-020-0058-6.
Hodson, A., Porter, P., Lowe, A., Mumford, P., 2002. Chemical denudation and silicate weathering in Himalayan glacier basins: Batura Glacier, Pakistan. J. Hydrol. 262 (1), 193–208. https://doi.org/10.1016/S0022-1694(02)00036-7.
Howard, A., 1994. A Detachment-Limited Model of drainage-basin evolution. Water Resour. Res. 30 (7), 2261–2285. https://doi.org/10.1029/94WR00757.
Hübner, H.M., 1986. Chapter 9 – Isotope effects of nitrogen in the soil and biosphere. Elsevier, pp. 361–425.
Ibarra, D.E., et al., 2016. Differential weathering of basaltic and granitic catchments from concentration–discharge relationships. Geochim. Cosmochim. Acta 190, 265–293. https://doi.org/10.1016/j.gca.2016.07.006.
Jacobson, A., Blum, J., 2000. Ca/Sr and $^{87}Sr/^{86}Sr$ geochemistry of disseminated calcite in Himalayan silicate rocks from Nanga Parbat: Influence on river-water chemistry. Geology 28. https://doi.org/10.1130/0091-7613(2000)28<463:SASGOD>2.0.CO;2.
Jacobson, A.D., Blum, J.D., Chamberlain, C.P., Poage, M.A., Sloan, V.F., 2002. Ca/Sr and Sr isotope systematics of a Himalayan glacial chronosequence: carbonate versus silicate weathering rates as a function of landscape surface age. Geochim. Cosmochim. Acta 66 (1), 13–27. https://doi.org/10.1016/S0016-7037(01)00755-4.
Jacobson, A.D., Blum, J.D., Chamberlain, C.P., Craw, D., Koons, P.O., 2003. Climatic and tectonic controls on chemical weathering in the New Zealand Southern Alps. Geochim. Cosmochim. Acta 67 (1), 29–46. https://doi.org/10.1016/S0016-7037(02)01053-0.
Jacobson, A.D., Grace Andrews, M., Lehn, G.O., Holmden, C., 2015. Silicate versus carbonate weathering in Iceland: New insights from ca isotopes. Earth Planet. Sci. Lett. 416, 132–142. https://doi.org/10.1016/j.epsl.2015.01.030.
Jiang, H., et al., 2018. Chemical weathering of small catchments on the Southeastern Tibetan Plateau I: Water sources, solute sources and weathering rates. Chem. Geol. 500, 159–174. https://doi.org/10.1016/j.chemgeo.2018.09.030.
Johnson, N.M., Reynolds, R.C., Likens, G.E., 1972. Atmospheric Sulfur: its effect on the Chemical Weathering of New England. Science 177 (4048), 514–516. https://doi.org/10.1126/science.177.4048.514.
Kanzaki, Y., Brantley, S.L., Kump, L.R., 2020. A numerical examination of the effect of sulfide dissolution on silicate weathering. Earth Planet. Sci. Lett. 539, 116239 https://doi.org/10.1016/j.epsl.2020.116239.
Karlsson, N., et al., 2021. A first constraint on basal melt-water production of the Greenland ice sheet. Nat. Commun. 12, 3461. https://doi.org/10.1038/s41467-021-23739-z.
Keene, W., Pszenny, A., Galloway, J., Hawley, M., 1986. Sea salt correction and interpretation of constituent ratios in marine precipitation. J. Geophys. Res. 91, 6647–6658. https://doi.org/10.1029/JD091iD06p06647.
Kemeny, P.C., et al., 2021. Sulfate sulfur isotopes and major ion chemistry reveal that pyrite oxidation counteracts CO_2 drawdown from silicate weathering in the Langtang-Trisuli-Narayani River system, Nepal Himalaya. Geochim. Cosmochim. Acta 294, 43–69. https://doi.org/10.1016/j.gca.2020.11.009.
Kendall, C., 1998. Chapter 16 – Tracing nitrogen sources and cycling in catchments. Elsevier, pp. 519–576.
Lal, R., 2001. World cropland soils as a source or sink for atmospheric carbon. Adv. Agron. 71 https://doi.org/10.1016/S0065-2113(01)71014-0.
Lasaga, A.C., Soler, J.M., Ganor, J., Burch, T.E., Nagy, K.L., 1994. Chemical weathering rate laws and global geochemical cycles. Geochim. Cosmochim. Acta 58 (10), 2361–2386. https://doi.org/10.1016/0016-7037(94)90016-7.
Lerman, A., Wu, L., Mackenzie, F.T., 2007. CO_2 and H_2SO_4 consumption in weathering and material transport to the ocean, and their role in the global carbon balance. Mar. Chem. 106 (1), 326–350. https://doi.org/10.1016/j.marchem.2006.04.004.
Li, H., et al., 2018. Spatiotemporal distribution and national measurement of the global carbonate carbon sink. Sci. Total Environ. 643, 157–170. https://doi.org/10.1016/j.scitotenv.2018.06.196.
Li, C., et al., 2019a. Estimation of carbonate rock weathering-related carbon sink in global major river basins. Acta Geograph. Sin. 74 (7), 1319–1332. https://doi.org/10.11821/dlxb201907004.
Li, H., Wang, S., Bai, X., Cao, Y., Wu, L., 2019b. Spatiotemporal evolution of carbon sequestration of limestone weathering in China. Sci. China Earth Sci. 62 (6), 974–991. https://doi.org/10.1007/s11430-018-9324-2.
Li, C., et al., 2022. High-resolution mapping of the global silicate weathering carbon sink and its long-term changes. Glob. Chang. Biol. 28 (14), 4377–4394. https://doi.org/10.1111/gcb.16186.
Liu, J., Han, G., 2020. Major ions and $\delta^{34}S_{SO4}$ in Jiulongjiang River water: investigating the relationships between natural chemical weathering and human perturbations. Sci. Total Environ. 724, 138208 https://doi.org/10.1016/j.scitotenv.2020.138208.
Liu, W., et al., 2016a. Chemical and strontium isotopic characteristics of the rivers around the Badain Jaran Desert, Northwest China: implication of river solute origin and chemical weathering. Environ. Earth Sci. 75 (15), 1119. https://doi.org/10.1007/s12665-016-5910-0.
Liu, W., et al., 2016b. Water geochemistry of the Qiantangjiang River, East China: Chemical weathering and CO_2 consumption in a basin affected by severe acid deposition. J. Asian Earth Sci. 127, 246–256. https://doi.org/10.1016/j.jseaes.2016.06.010.
Liu, W., et al., 2018. Geochemistry of the dissolved loads during high-flow season of rivers in the southeastern coastal region of China: anthropogenic impact on chemical weathering and carbon sequestration. Biogeosciences 15 (16), 4955–4971. https://doi.org/10.5194/bg-15-4955-2018.
Liu, W., et al., 2022. Lithological and glacial controls on sulfide weathering and the associated CO_2 budgets in the Tibetan Plateau: New constraints from small catchments. Geochim. Cosmochim. Acta. https://doi.org/10.1016/j.gca.2022.12.015.
Lourakis, M., 2005. A Brief Description of the Levenberg-Marquardt Algorithm Implemened by Levmar. Institute of Computer Science, Foundation for Research and Technology, p. 4.
Louvat, P., Gislason, S., Allegre, C., 2008. Chemical and mechanical erosion rates in Iceland as deduced from river dissolved and solid material. Am. J. Sci. 308, 679–726. https://doi.org/10.2475/05.2008.02.
Macdonald, F.A., Swanson-Hysell, N.L., Park, Y., Lisiecki, L., Jagoutz, O., 2019. Arc-continent collisions in the tropics set Earth's climate state. Science 364 (6436), 181. https://doi.org/10.1126/science.aav5300.
Mackenzie, F., Garrels, R., 1971. Evolution of Sedimentary Rocks, 101. Norton, New York.
Maffre, P., et al., 2018. Mountain ranges, climate and weathering. Do orogens strengthen or weaken the silicate weathering carbon sink? Earth Planet. Sci. Lett. 493, 174–185. https://doi.org/10.1016/j.epsl.2018.04.034.
Maher, K., Chamberlain, C.P., 2014. Hydrologic regulation of chemical weathering and the geologic carbon cycle. Science 343 (6178), 1502. https://doi.org/10.1126/science.1250770.
Marquardt, D.W., 1963. An algorithm for least-squares estimation of nonlinear parameter. J. Soc. Ind. Appl. Math. 11, 431–441. https://doi.org/10.1137/0111030.
Mast, M.A., Drever, J.I., Baron, J., 1990. Chemical weathering in the Loch Vale Watershed, Rocky Mountain National Park, Colorado. Water Resour. Res. 26 (12), 2971–2978. https://doi.org/10.1029/WR026i012p02971.
Meybeck, M., 1987. Global chemical weathering of surficial rocks estimated from river dissolved loads. Am. J. Sci. 287 (5), 401–428. https://doi.org/10.2475/ajs.287.5.401.
Milliman, J.D., 1995. River Discharge to the Sea a Global River Index (GLORI). IGBP-LOICZ Report, 125 pp.
Millot, R., Gaillardet, J., Dupré, B., Allègre, C.J., 2002. The global control of silicate weathering rates and the coupling with physical erosion: new insights from rivers of the Canadian Shield. Earth Planet. Sci. Lett. 196 (1), 83–98. https://doi.org/10.1016/S0012-821X(01)00599-4.
Mitchell, A.C., Brown, G.H., 2008. Modeling Geochemical and Biogeochemical Reactions in Subglacial Environments. Arct. Antarct. Alp. Res. 40 (3), 531–547. https://doi.org/10.1657/1523-0430(06-075)[MITCHELL]2.0.CO;2.
Moon, S., Huh, Y., Qin, J., Pho, N., 2007. Chemical weathering in the Hong (Red) river basin: rates of silicate weathering and their controlling factors. Geochim. Cosmochim. Acta 71, 1411–1430. https://doi.org/10.1016/j.gca.2006.12.004.
Moon, S., Chamberlain, C.P., Hilley, G.E., 2014. New estimates of silicate weathering rates and their uncertainties in global rivers. Geochim. Cosmochim. Acta 134, 257–274. https://doi.org/10.1016/j.gca.2014.02.033.
Moore, J., Jacobson, A.D., Holmden, C., Craw, D., 2013. Tracking the relationship between mountain uplift, silicate weathering, and long-term CO_2 consumption with Ca isotopes: Southern Alps, New Zealand. Chem. Geol. 341, 110–127. https://doi.org/10.1016/j.chemgeo.2013.01.005.
Moosdorf, N., Hartmann, J., Lauerwald, R., Hagedorn, B., Kempe, S., 2011. Atmospheric CO_2 consumption by chemical weathering in North America. Geochim. Cosmochim. Acta 75 (24), 7829–7854. https://doi.org/10.1016/j.gca.2011.10.007.
Moquet, J.S., et al., 2011. Chemical weathering and atmospheric/soil CO_2 uptake in the Andean and Foreland Amazon basins. Chem. Geol. 287, 1–26. https://doi.org/10.1016/j.chemgeo.2011.01.005.
Navarre-Sitchler, A., Brantley, S., 2007. Basalt weathering across scales. Earth Planet. Sci. Lett. 261 (1), 321–334. https://doi.org/10.1016/j.epsl.2007.07.010.
Oliva, P., Viers, J., Dupré, B., 2003. Chemical weathering in granitic environments. Chem. Geol. 202 (3), 225–256. https://doi.org/10.1016/j.chemgeo.2002.08.001.
Oliva, P., Dupré, B., Martin, F., Viers, J., 2004. The role of trace minerals in chemical weathering in a high-elevation granitic watershed (Estibère, France): chemical and mineralogical evidence1 1Associate editor: S. Krishnaswami. Geochim. Cosmochim. Acta 68 (10), 2223–2243. https://doi.org/10.1016/j.gca.2003.10.043.
Peel, M., Finlayson, B., McMahon, T., 2007. Updated world map of the Koppen-Geiger climate classification. Hydrol. Earth Syst. Sci. Discuss. 4 https://doi.org/10.5194/hess-11-1633-2007.
Perrin, A.-S., Probst, A., Probst, J.-L., 2008. Impact of nitrogenous fertilizers on carbonate dissolution in small agricultural catchments: Implications for weathering CO_2 uptake at regional and global scales. Geochim. Cosmochim. Acta 72 (13), 3105–3123. https://doi.org/10.1016/j.gca.2008.04.011.
Relph, K.E., et al., 2021. Partitioning riverine sulfate sources using oxygen and sulfur isotopes: Implications for carbon budgets of large rivers. Earth Planet. Sci. Lett. 567, 116957 https://doi.org/10.1016/j.epsl.2021.116957.
Riebe, C.S., Kirchner, J.W., Granger, D.E., Finkel, R.C., 2001. Strong tectonic and weak climatic control of long-term chemical weathering rates. Geology 29 (6), 511–514. https://doi.org/10.1130/0091-7613(2001)029<0511:STAWCC>2.0.CO;2.
Riebe, C.S., Kirchner, J.W., Finkel, R.C., 2004. Erosional and climatic effects on long-term chemical weathering rates in granitic landscapes spanning diverse climate

regimes. Earth Planet. Sci. Lett. 224 (3), 547–562. https://doi.org/10.1016/j.epsl.2004.05.019.
Sherwood, W., 1989. Chloride Loading in the South Fork of the Shenandoah River, Virginia, U.S.a. Environ. Geol. Water Sci. 14, 99–106. https://doi.org/10.1007/BF01728501.
Smith, P., et al., 2008. Greenhouse gas mitigation in agriculture. Philos. Trans. R. Soc. Lond. Ser. B Biol. Sci. 363 (1492), 789–813. https://doi.org/10.1098/rstb.2007.2184.
Spence, J., Telmer, K., 2005. The role of sulfur in chemical weathering and atmospheric CO_2 fluxes: evidence from major ions, $\delta^{13}C_{DIC}$, and $\delta^{34}S_{SO4}$ in rivers of the Canadian Cordillera. Geochim. Cosmochim. Acta 69 (23), 5441–5458. https://doi.org/10.1016/j.gca.2005.07.011.
Sverdrup, H., Warfvinge, P., 1995. Estimating field weathering rates using laboratory kinetics. Rev. Mineral. Geochem. 31 (1), 485–541. https://doi.org/10.1515/9781501509650-013.
Syvitski, James P.M., Milliman, John D., 2007. Geology, geography, and Humans Battle for dominance over the delivery of Fluvial Sediment to the Coastal Ocean. J. Geol. 115 (1), 1–19. https://doi.org/10.1086/509246.
Tao, Z., et al., 2011. Estimation of carbon sinks in chemical weathering in a humid subtropical mountainous basin. Chin. Sci. Bull. 56, 3774–3782. https://doi.org/10.1007/s11434-010-4318-6.
Taylor, A.S., Blum, J.D., Lasaga, A.C., MacInnis, I.N., 2000. Kinetics of dissolution and Sr release during biotite and phlogopite weathering. Geochim. Cosmochim. Acta 64 (7), 1191–1208. https://doi.org/10.1016/S0016-7037(99)00369-5.
Taylor, L., et al., 2015. Enhanced weathering strategies for stabilizing climate and averting ocean acidification. Nat. Clim. Chang. 6 https://doi.org/10.1038/nclimate2882.
Terrer, C., et al., 2021. A trade-off between plant and soil carbon storage under elevated CO_2. Nature 591, 599–603. https://doi.org/10.1038/s41586-021-03306-8.
Tipper, E.T., et al., 2006. The short term climatic sensitivity of carbonate and silicate weathering fluxes: Insight from seasonal variations in river chemistry. Geochim. Cosmochim. Acta 70 (11), 2737–2754. https://doi.org/10.1016/j.gca.2006.03.005.
Tipper, E.T., et al., 2021. Global silicate weathering flux overestimated because of sediment–water cation exchange. Proc. Natl. Acad. Sci. 118 (1), e2016430118 https://doi.org/10.1073/pnas.2016430118.
Torres, M.A., West, A.J., Li, G., 2014. Sulphide oxidation and carbonate dissolution as a source of CO_2 over geological timescales. Nature 507 (7492), 346–349. https://doi.org/10.1038/nature13030.
Torres, M.A., et al., 2016. The acid and alkalinity budgets of weathering in the Andes–Amazon system: Insights into the erosional control of global biogeochemical cycles. Earth Planet. Sci. Lett. 450, 381–391. https://doi.org/10.1016/j.epsl.2016.06.012.
Tranter, M., et al., 2002. Geochemical weathering at the bed of Haut Glacier d'Arolla, Switzerland—a new model. Hydrol. Process. 16 (5), 959–993. https://doi.org/10.1002/hyp.309.
Vicca, S., et al., 2022. Is the climate change mitigation effect of enhanced silicate weathering governed by biological processes? Glob. Chang. Biol. 28 (3), 711–726. https://doi.org/10.1111/gcb.15993.
Walker, J., Hays, P., Kasting, J., 1981. A negative feedback mechanism for the long-term stabilization of Earths surface-temperature. J. Geophys. Res.-Atmos. 86, 9776–9782. https://doi.org/10.1029/JC086iC10p09776.
Wang, G., Dai, M., Shen, S., Bai, Y., Xu, Y., 2014. Quantifying uncertainty sources in the gridded data of sea surface CO_2 partial pressure. J. Geophys. Res. Oceans 119. https://doi.org/10.1002/2013JC009577.
West, A.J., 2012. Thickness of the chemical weathering zone and implications for erosional and climatic drivers of weathering and for carbon-cycle feedbacks. Geology 40, 811–814. https://doi.org/10.1130/G33041.1.
White, A.F., Bullen, T.D., Vivit, D.V., Schulz, M.S., Clow, D.W., 1999. The role of disseminated calcite in the chemical weathering of granitoid rocks. Geochim. Cosmochim. Acta 63 (13), 1939–1953. https://doi.org/10.1016/S0016-7037(99)00082-4.
White, A.F., Schulz, M.S., Lowenstern, J.B., Vivit, D.V., Bullen, T.D., 2005. The ubiquitous nature of accessory calcite in granitoid rocks: Implications for weathering, solute evolution, and petrogenesis. Geochim. Cosmochim. Acta 69 (6), 1455–1471. https://doi.org/10.1016/j.gca.2004.09.012.
Wilson, T.R.S., 1975. Salinity and the major elements of sea water. In: Riley, J.P., Skirrow, G. (Eds.), Chemical Oceanography: Salinity and the Major Elements of Sea Water. Academic Press, New York, pp. 365–413.
Wolfgang, D., 2012. Processes in Karst Systems: Physics, Chemistry, and Geology.
Worthington, S.R.H., Davies, G.J., Alexander, E.C., 2016. Enhancement of bedrock permeability by weathering. Earth Sci. Rev. 160, 188–202. https://doi.org/10.1016/j.earscirev.2016.07.002.
Xiao, B., et al., 2023. Responses of carbon and water use efficiencies to climate and land use changes in China's karst areas. J. Hydrol. 617, 128968 https://doi.org/10.1016/j.jhydrol.2022.128968.
Xiong, L., et al., 2022. High-resolution data sets for global carbonate and silicate rock weathering carbon sinks and their change trends. Earth's Future 10 (8), e2022EF002746. https://doi.org/10.1029/2022EF002746.
Xu, S., et al., 2021. Oxidation of pyrite and reducing nitrogen fertilizer enhanced the carbon cycle by driving terrestrial chemical weathering. Sci. Total Environ. 768, 144343 https://doi.org/10.1016/j.scitotenv.2020.144343.
Zeng, S., Liu, Z., Groves, C., 2022. Large-scale CO_2 removal by enhanced carbonate weathering from changes in land-use practices. Earth Sci. Rev. 225, 103915 https://doi.org/10.1016/j.earscirev.2021.103915.
Zhang, X., et al., 2019. Hydro-Geochemical and Sr Isotope Characteristics of the Yalong River Basin, Eastern Tibetan Plateau: Implications for Chemical Weathering and Controlling Factors. Geochem. Geophys. Geosyst. 20 (3), 1221–1239. https://doi.org/10.1029/2018GC007769.
Zhang, S., et al., 2021. Global CO_2 Consumption by Silicate Rock Chemical Weathering: its past and Future. Earth's Future 9 (5), e2020EF001938. https://doi.org/10.1029/2020EF001938.